Jour. Korean Earth Science Society, v. 24, no. 1, p. 7–21, January 2003

Sea State Hindcast for the Korean Seas With a Spectral Wave Model and Validation with Buoy Observation During January 1997

B. Prasad Kumar[1], Ig-Chan Pang[2,*], A.D. Rao[1], Tae-Hee Kim[3], Jae-Cheol Nam[3], and Chang-Su Hong[2]

[1]Centre for Atmospheric Sciences, Indian Institute of Technology Delhi, New Delhi 110 016, India
[2]Department of Oceanography, Cheju National University, Korea
[3]Marine Meteorological & Earthquake Research Laboratory,
Meteorological Research Institute (METRI), Korea Meteorology Administration (KMA)

Abstract : The state-of-art third generation wave prediction model WAM was applied to the Korean seas for a winter monsoon period of January 1997. The wind field used in the present study is the global NSCAT-ERS/NCEP blended winds, which was further interpolated using a bi-cubic spline interpolator to fine grid limited area shallow water regime surrounding the Korean seas. To evaluate and investigate the accuracy of WAM, the hindcasted wave heights are compared with observed data from two shallow water buoys off Chil-Bal and Duk-Juk. A detailed study has been carried with the various meteorological parameters in observed buoy data and its inter-dependency on model computed wave fields was also investigated. The RMS error between the observation and model computed wave heights results to 0.489 for Chil-Bal and 0.417 for Duk-Juk. A similar comparison between the observation and interpolated winds off Duk-Juk show RMS error of 2.28 which suggest a good estimate for wave modelling studies.

Keywords : spectral wave model, model validation, sea state hindcast, buoy obserbation, Korean sea

Introduction

Wave modelling is an art of deriving the wave conditions at a given time and location, starting from the essential information of the wind and geometry of the basin. At present we can identify two main directions of interest in wave modelling. Firstly the global view of the problem, which is connected to the use of satellite data and long term climatological problems. The second one follows the high density of humanity and economical interests on the coasts of various continents, focussing on aspects related more to the smaller scale in time and space, of processes involved in coastal areas and regional seas. In our present study, we deal the latter focussing attention on the regional seas around the Korean peninsula.

The Korean peninsula protrudes southward from the Asian mainland seperating the Yellow Sea (West Sea) to the West and Sea of Japan (East Sea) to its East. The peninsula is roughly 346 Km wide at its broadest point which lie approximately at 38°10'N, and roughly 169 Km at its narrowest point which is approximately located at 39°20'N and approximately 965 Km long. The northern most point of the peninsula is located on the China border which is approximately 43°N. The Western most point on the peninsula is located at 124°40'E on the Yellow Sea, and the eastern most point on the peninsula is located at 129°35'E on the Sea of Japan.

Korea is located in the East Asian Monsoon belt. Seasonal monsoon winds affect the weather in the peninsula throughout the year. The Southwest monsoon wind blows both from the South and Southeast during the summer months and the Northeast monsoon from North and North-west during the winter months (November-March). The wind system is stronger in the winter months compared to the summer months. In the present study wave hindcast was performed for the winter month of January 1997. The study region emcompass the

*E-mail: Pangig@cheju.cheju.ac.kr

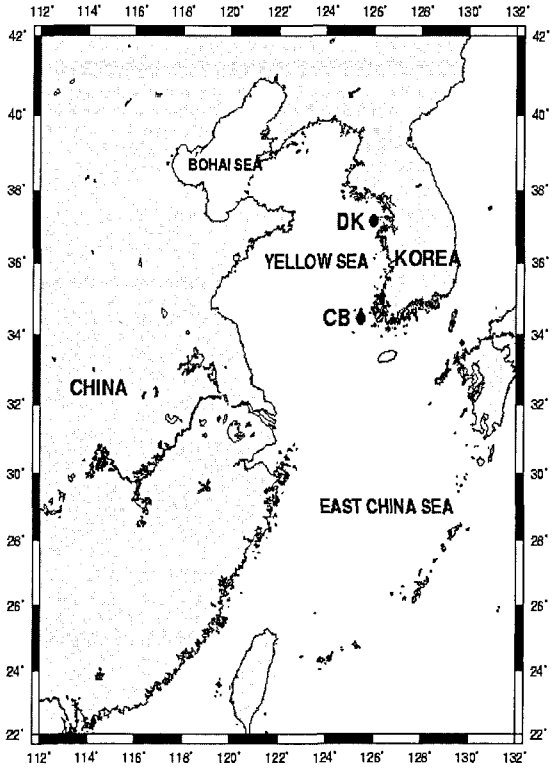

Fig. 1. Study region with location of shallow water buoys.

Gulf of Bohai, the Yellow Sea and the East China Sea. Numerical experiments were performed applying the WAM model to this study region and validation carried out for two shallow water points located in the Yellow Sea.

Formulation

Characteristics of the Yellow Sea

The Yellow Sea is a marginal sea between China and Korea (Fig. 1). This sea between the Bohai Sea and the East China Sea has a maximum depth of 103 m and an average depth of 44 m. The Bohai sea is a shallow bay region north of the Yellow Sea. The East China Sea lie between the Yellow Sea and the Ryukyu Islands. Oceanographical conditions of the Yellow Sea is characerized by high tides, seasonally varying monsoon, fresh water discharge from surrounding land masses and the Kuroshio current system. Seas around the Korean peninsula are characterized by high tides, high waves with perennial typhoon attacks. Unlike the Yellow Sea, the East China Sea has steep topographic gradients with water depths exceeding 2000 m. Within 50 Km of the western Korean coastline the average water depth is less than 20 m.

Two factors determine the characteristics of the East China Sea and the Yellow Sea. First is their proximity to the Kuroshio and next is the monsoon winds which bring Northerly winds during winter and Southerly/South-easterly winds during summer to the entire region. The Yellow Sea region is prevailed by strong Northerly (NNE-NW) monsoon from late November to March where the average velocity in January is about 10 ms^{-1} (Yuan and Su, 1984). This corresponds to the steep pressure gradient between the Siberian High which covers most of the Asian continent, and the Aleutian Low which covers the northern most part of the Pacific Ocean. The mean wind speed reaches a maximum in February with an average of 3.5 ms^{-1} near the central portion and of 2.8 ms^{-1} over the whole Yellow Sea (Elms, 1990). April is the period of alternating monsoon when the wind blows onshore with velocities around 1.5 ms^{-1}.

Formulation of the Model

The evolution of two dimensional ocean wave spectra E (f,θ,x,t) in the form of energy balance equation can be expressed in the form:

$$\partial E/\partial t + C_g \cdot \nabla E = S \quad (1)$$

E is the energy component of frequency, f (Hz) and direction (θ). C_g is the group velocity of spectral component and S describes the sources and sinks by which the energy is gained or lost by a spectral component travelling at its group velocity. Referring to equation (1), the group velocity C_g and direction of propagation (q) are time dependent when following a parcel of wave energy in presence of variable water depth. Following Golding (1983) the appropriate expansion is:

$$dE/dt \equiv \partial E/\partial t + \nabla \cdot (C_g E) + \partial\{(C_g \cdot \nabla\theta)E\}/\partial\theta \quad (2)$$

The second term in the right hand side represents propagation and third term describes refraction. The function S in equation (1) may be expanded (Hasselmann, 1973) as:

$$S = S_{in} + S_{nl} + S_{ds} + S_{bot} \quad (3)$$

where, S_{in} represents energy input from the atmosphere (mainly winds), S_{nl} redistribution of energy within the wave spectrum due to non-linear interactions. S_{ds} energy loss due to white capping and dissipation and S_{bot} the energy loss in shallow water due to bottom interaction. Combining equations (2) and (3) the energy balance equation (1) can be rewritten as:

$$\partial E/\partial t = -\nabla \cdot (C_g E) - \partial\{(C_g \cdot \nabla\partial)E\}/\partial\theta + S_{in} + S_{nl} + S_{ds} + S_{bot} \quad (4)$$

Equation (4) is solved numerically. Assuming that a wave may reach its fully developed stage, for a pre-determined time step (Δt), grid spacing is decided by the condition $\Delta x \geq C_g \Delta t$ where C_g is the group velocity.

The frequencies in WAM ranges from 0.0418 Hz to 0.4114 Hz in a geometric progression with a common ratio of 1.1, and directional component of 30 bands with an angular resolution of 12°. Two alternative propagation schemes were implemented in this model, which being a first order upwind scheme and a second order leap frog scheme (WAMDI Group, 1988). Refraction due to variations in water depth has been treated in WAM by the great circle propagation relation proposed by Groves and Melcer (1961).

As mentioned in the energy balance equation (4) there are four source terms. These four terms interact with each other thereby bringing up a resultant energy balance. The source term (S_{in}) represents the energy input from the atmosphere which is mainly due to winds and is always positive. The non-linear wave-wave interaction (S_{nl}) follows the discrete interaction approximation theory proposed by Hasselmann and Hasselmann (1985) and Hasselmann *et al.* (1985). The dissipation due to whitecapping (S_{ds}) and wave breaking is a sink (negative) mechanism. S_{bot} is a sink (negative) mechanism.

As wave grows, energy growth develops from the high frequency region and migrates towards lower frequencies. With an increase in wind speed, peak frequency displaces to lower frequencies. The relative shift in the peak frequency (f_p) obeys an empirical relation for a fully developed sea which being $f_p U = 2.467$. In WAM the energy input (S_{in}) is represented by an exponential term following Miles (1957,1960) which was expressed in the form:

$$S_{in} = \beta E \quad (5)$$

The exponential term (b) as proposed by Snyder (1981) is given by:

$$\beta = \max\left\{0., 0.25\frac{\rho_a}{\rho_w}\left(28\frac{u^*}{c}\cos\theta_w - 1\right)\right\}\omega \quad (6)$$

where $\omega = 2\pi f$, ρ_a and ρ_w are air and water density, u_* the friction velocity, c the phase velocity and θ_w is the angle between wind and wave directions. S_{nl} represents the non linear conservative energy exchange associated by the possible quadruplets of wave components that satisfy a given resonance condition.

Wave dissipation occurs when waves break during wave generation and later as they approach a shoreline. In deep water wave breaking is generally visible in the form of white topped waves. Wave dissipation can be visualized as a limiting factor to fully developed spectrum of Pierson-Moskowitz (1964). The only way in doing this is to make dissipation explicitly balance the input when the fully developed stage is approached. Ewing (1971) applied this condition to each frequency components such that energy at any frequency does not exceed its fully developed value at any time during the growth. The final form of the

source term in WAM takes the form as proposed by Komen *et al.* (1984).

Interaction of waves with bottom is one of the dissipative mechanisms, represented by S_{bot} in the energy balance equation. The relative strength of the wave bottom interaction mechanism due to scattering on bottom irregularities, motion of a soft bottom, percolation and friction in a turbulent boundary layer was studied by Shemdin (1978). The first quantitative measurements of this phenomena was made during the JONSWAP experiments (Hasselmann, 1973) in which the damping factor in WAM was taken as $c_{df} = 0.038\ m^2 s^{-3}$.

Integration of the Source Parameters

An implicit second order centered difference scheme was applied in WAM to solve the energy balance equation. Keeping aside the advection term in the energy balance equation, the energy of the (n + 1)th time level can be expressed as:

$$E_{n+1} = E_n + \frac{\Delta t}{2}(S_{n+1} + S_n) \tag{7}$$

where Δt is the time step, and S represents the source function. Among these source terms, only the wind input term (S_{in}) is linear and the others are expanded using the Taylor expansion. For the wind input source term (S_{in}):

$$S^{in}_{n+1} = \beta_{n+1} E_{n+1} = \beta_{n+1} \Delta E + \beta_{n+1} E_n \tag{8}$$

$$\text{where, } \Delta E = E_{n+1} - E_n \tag{9}$$

The final form of the incremental energy change required for the next time step was:

$$\Delta E = \Delta t \left[\left(\frac{\beta_n + \beta_{n+1}}{2} \right) E_n + S_n^{rest} \right] \left[1 - \frac{\Delta t}{2}(A_n + \beta_{n+1}) \Delta E \right]^{-1} \tag{10}$$

the superscript 'rest' in equation (10) refers to the remaining source terms other than the wind input source.

Data and Methodology

Surface waves evolves from the direct effect of wind blowing over the sea surface. An error in the wind input field is reflected as an error in computation of the surface wave conditions. Wind waves are very sensitive to small variations in the input and in a fully developed situation the significant wave height is proportional to sqaure of the wind velocity. However, the spatial distribution of the errors is quite different in wind and the wave fields. Wind errors are normally concentrated in areas, close to orographic regions or close to a front. The wave conditions at a given point result from an integrated effect in space and time, of the previous winds blowing throughout the basin.

Normally the input winds for wave prediction come from a hindcast , an analysis, a forecast or an idealized case. Depending on the structure and the sophistication of the dynamics, wave models react differently to the same variations in the input wind fields. In case of state-of-art third generation WAM, used in this study, the intrinsic errors, due to approximation associated with the formulation of the wave model, seems to be smaller than the errors commonly present in the wind fields (Komen *et al.*, 1994). The SWADE experiments (Weller *et al.*, 1991) also clearly demonstrate the importance of specifying the surface meteorolgy with sufficient accuracy and spatial coverage and its impact on ocean wave modelling.

For the present study surface winds at a time interval of 6 h ($0.5^\circ \times 0.5^\circ$) were extracted for the Korean seas from the global 6 hourly maps of blended NSCAT/ERS with NCEP analysis (Milliff *et al.*, 1999) for the winter monsoon period of January 1997. The blending method creates the global wind field by retaining the NSCAT/ERS wind reteievals in swath regions, and in unsampled region (nadir and interswath gaps) augmenting the low wavenumber NCEP fields with a high wave

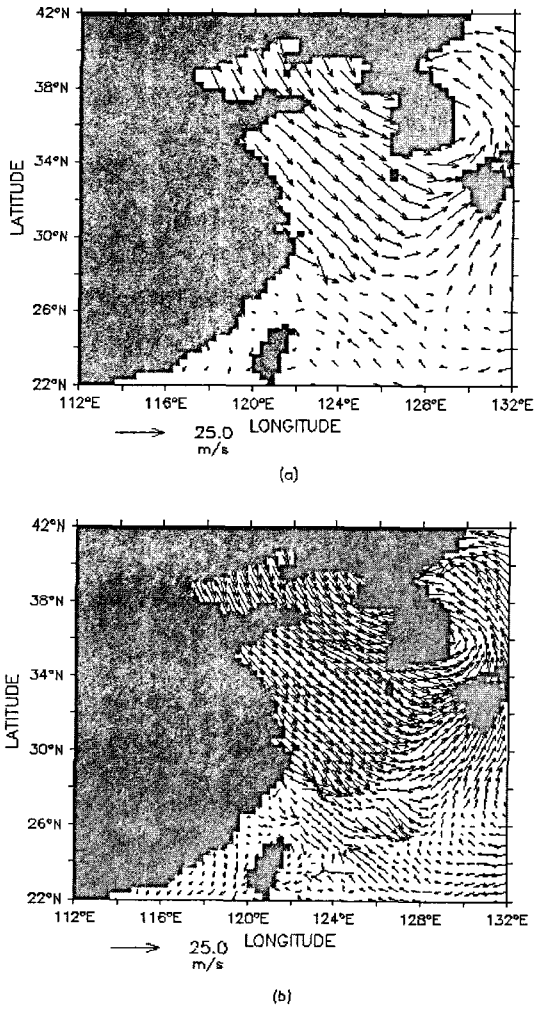

Fig. 2. Initial wind field on 1 January 1997 and the corresponding (b) interpolated wind field.

number component derived from monthly regional statistics. The details of the blending methodology are given in Chin *et al.* (1998). The 6 hourly retrieved $0.5^{\circ} \times 0.5^{\circ}$ wind fields were interpolated to $0.25^{\circ} \times 0.25^{\circ}$ bins using a standard bi-cubic spline interpolator. The study region which encompass the Bohai Sea, Yellow Sea and the East China Sea alongwith the location of two shallow water buoys which was used for validation in our present study is shown in Fig. 1. The initial wind field ($0.5^{\circ} \times 0.5^{\circ}$) as on 1st January 1997 and the interpolated wind field (0.25××0.25×) is represented in Fig. 2 (a,b) The latter is used for present study in forcing WAM during January 1997. The study region is a square domain 22°N - 42°N and 112°E - 132°E. The corresponding location of the two shallow water buoys are Duk-Juk (126.01°E, 37.14°N) and Chil-Bal (125.47°E, 34.48°N). Their corresponding water depths are 25 m off Duk-Juk and 75 m off Chil-Bal. The model was run from a cold start with the initial spectra of JONSWAP. The bathymetry for the study region was extracted from 5 global bathymetry data of National Geophysical Data Centre (NGDC).

Results and Discussion

The mean wave height during January 1997 for Chil-Bal and Duk-Juk is shown in Fig. 3 (a,b). The figure shows the comparison in mean wave height between the WAM model and the observations recorded by buoy both at (a) Chil-Bal and (b) Duk-Juk at an interval of 12 hours starting from 1st January 1997. As seen from Fig. 3 (a,b) mean wave heights in the order of 6.2 m at Chil-Bal and 3.2 m at Duk-Juk during 1st January 1997 is that associated with a depression which occurred in Korean seas during the end of December 1996. The model computed mean wave heights were seen closely following the buoy observations at both these locations. Significant peaks in mean wave heights were noticed during 5th, 13th, 21st and 28th January 1997 both at Chil-Bal and Duk-Juk. Maximum sustained winds were noticed about 14.5 ms^{-1} off Chil-Bal and 17.8 ms^{-1} off Duk-Juk respectively during this period as dipicted in Fig. 4 (a,b). The significant peak wave heights are also noticed at an interval of about eight days (Fig. 4 a,b). Moreover, the bouy data for at Chil Bal (Fig. 4a) is also following the same pattern as that of NSCAT/NCEP wind data. However, at Duk-Juk, the bouy data is not available (Fig. 4b). A critical study on the quantitative nature of the oscillation found in the wind magnitude as evidenced from buoy observations at both these locations will be useful to

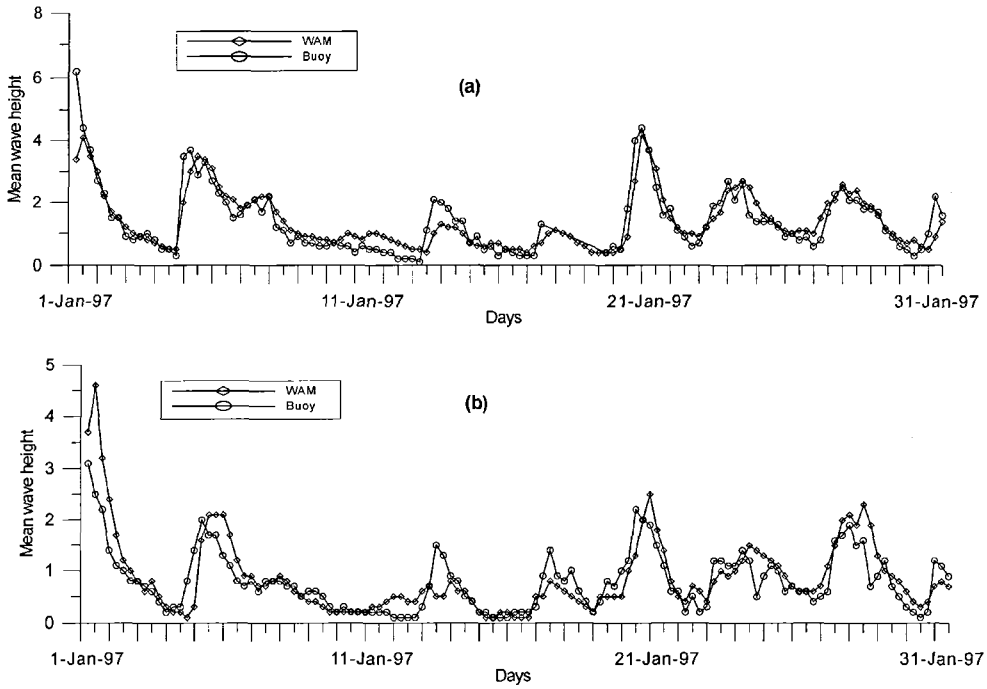

Fig. 3. Comparison of mean wave height from WAM and buoy observation off (a) Chil-Bal and (b) Duk-Juk during January 1997.

improve the quality of forecast in the existing wind models, resulting in better wave forecast in the Korean seas. Table 1 shows the correlation coefficient and RMS error of wave height and surface winds between observation and model for the two stations. A comparitative study on wind and wave directions with the NSCAT/NCEP blended winds against the buoy observations is highlighted for Chil-Bal (Fig. 5a,b) and Duk-Juk (Fig. 6a,b). In Fig. 5 (a), the predominant wind direction was found north-easterly during January 1997 off Chil-Bal. The predominant wave direction for Chil-Bal is north-easterly which is almost synchronous with the collated wind directions. The WAM model computed wave direction closely resembles the buoy wave direction. It could be noticed from Fig. 5(b), the dominant wave direction is North-Easterly for wave heights less than 2 m. The angular spread in bouy wave direction was seen shiifting towards northerly for wave heights more than 2m. In case of Duk-Juk (Fig. 6a), the wind direction of NSCAT/NCEP blended winds was found centered in the North-Westerly direction which is analogous to climatological pattern. It is observed that the stronger winds mostly follow climatological pattern at both the stations (Fig. 5a, 6a). As in Fig. 6b, close resemblence between model wave direction and buoy observed wave direction is noticed. This is in contrast to that of Fig. 5b. As in Fig. 5b, some isolated observations are noticed in different directions which may be due to wave reflection commonly noticed in the shallow waters. The wave direction is predominantly westerly for the wave heights less than 1 m. However, as it is seen in Fig. 5b, the WAM wave direction is shifting towards right of the buoy wave direction for the wave heights larger than 1 m. The winds at Chil-Bal are stronger and hence produce larger wave heights. These larger waves with passage of time gets transformed into swell waves whose amplitudes are relatively small compared to wind waves. These swells may be seen reaching Duk-Juk from southwest. To assess the oscillations evidenced from the wind speeds (Fig. 4a,b) at both the locations, the

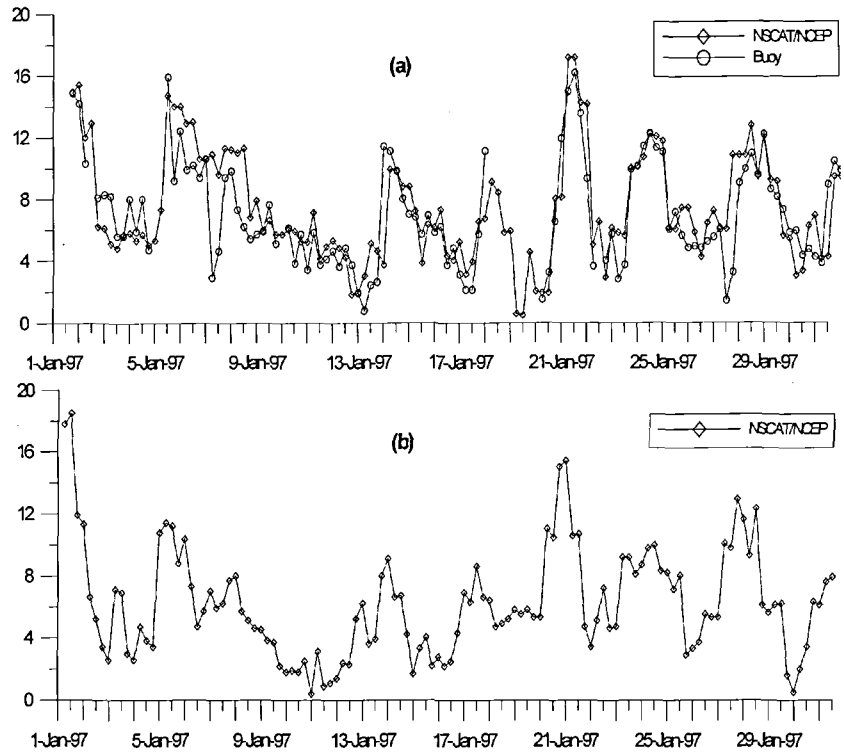

Fig. 4. Comparison of NSCAT/NCEP blended winds with buoy wind speed off (a) Chil-Bal and (b) Duk-Juk.

Table 1. Correlation coefficient and RMS error of wave height and sea surface wind speeds

Station	Wave height (m)		Wind speed (m/s)	
	Correlation coeff.	RMSE	Correlation coeff.	RMSE
Duk-Juk	0.83464	0.41734	0.80093	2.2837
Chil-Bal	0.891746	0.48962	***	***

***indicate missing value in buoy record

pressure field, air-temperature and SST obtained from buoy observations have been studied at Chil-Bal and Duk-Juk as shown in Fig. 7. From Fig. 7a, it is noticed that the low-pressure exists on 5th, 13th, 21st and 28th respectively. These low-pressure events are associated with high winds which are observed both in NSCAT and bouy data. The temporal distribution of air temperature and SST for Chil-Bal is shown in Fig. 7(b,c). Sharp variations in air temperature were noticed on 5th, 13th, 21st and 28th January 1997 off Chil-Bal. Lowering of air temperature were noticed on 5th ($\approx$0°) and 21st ($\approx$0°) January 1997 while it is higher on 13th ($\approx$8°) and 28th ($\approx$8°) during the period January 1997. The higher air-temperature is associated with lowering of surface pressure and vice-versa. The SST trend is similar at both the stations but the coastal waters at Duk-Juk are more warm. The SST is noticed in general having a downward trend during January.

In order to substantiate the findings in the surface pressure distribution off Chil-Bal and Duk-Juk, we study the synoptic charts of Korea Meteorological Administration (KMA) from 18-22 January 1997 which is available at a time interval of 12 h as dipicted in Fig. 8 (a-i). The overall observation from the synoptic charts reveals complex synoptic features with multiple high and low pressure systems distributed randomly in the Korean

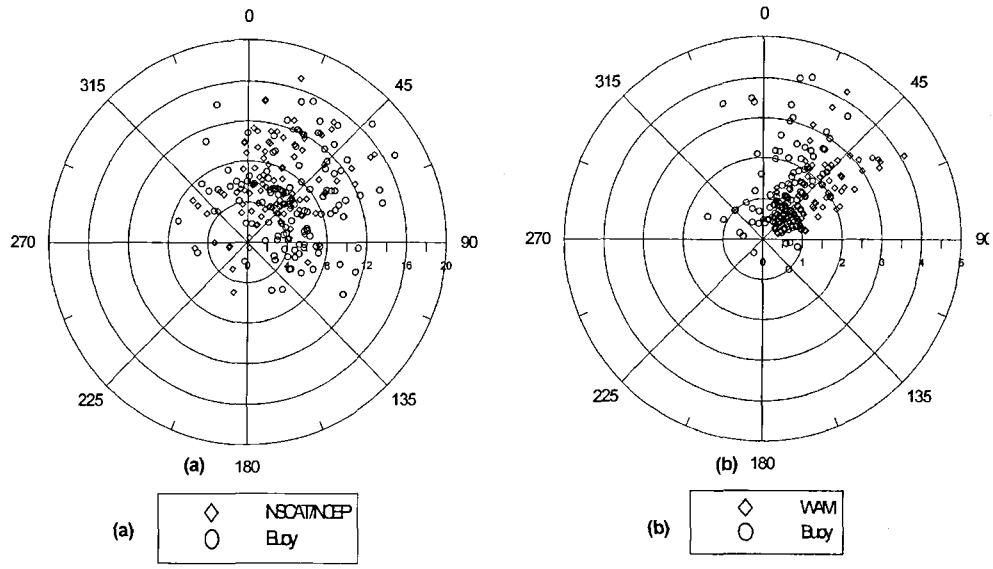

Fig. 5. Comparison of (a) NSCAT/NCEP blended wind direction and (b) WAM wave direction with Buoy wave direction off Chil-Bal.

seas. These systems are seen as fast response with reference to time. However, in this case study the movement of pressure patterns was made with reference to the two observational locations (hereafter referred to as "O"). At 1800 UTC a strong high pressure system (as seen by the closeness of isobars) was observed west of "O" with a core of 1056 hPa. The outer periphery of this system was seen occupying the study area with a surface pressure of 1024 hPa. Simultaneously, two low pressure systems lie centered in the north-east sector and a high pressure area to the north of "O". The observed high pressure system was seen migrating towards "O" by 1812 UTC where the surface pressure were 1024 hPa at "O". Strengthening of the low pressure on the north-east sector was also observed during this period. The influence of the low pressure system had reduced the surface pressure to 1020 hPa at "O" on 1900 UTC. The growth of the high pressure system found during 1800 UTC was seen extending towards "O" resulting in surface pressure of 1020 hPa at 1912 UTC. The intensity of the low system was seen with the same factor as during 1900 UTC. Waning of the low system was also seen progressing further north-east and the northerly distributed high pressure system was seen intensifying further resulting in surface pressure of 1020 hPa at both locations of "O" on 2000 UTC. An interesting observation was seen during 2012 UTC where the already intensified high pressure system north of "O" was found migrating towards the region where north-east low is located. This has resulted in variable surface pressure distribution at "O" which was observed as 1020 hPa off Chil-Bal and 1022 hPa off Duk-Juk. A similar sort of surface pressure distribution was noticed during 2100 UTC with a notable increase in the intensity of the low pressure system. However, the surface pressure at these locations were as seen during 2012 UTC. In the two cells noticed in the low pressure system which was seen from 1800 UTC till 2012 UTC, one of the low cell was seen moving southerly. This resulted in a surface pressure of 1024 hPa off Chil-Bal and 1028 hPa off Duk-Juk. The higher surface pressure off Duk-Juk was associated with the already present high northwest off Duk-Juk. Further intensification in the southerly component of the low pressure cell was observed during 2200 UTC and rapid migration of the high towards north off Duk-Juk was also seen.

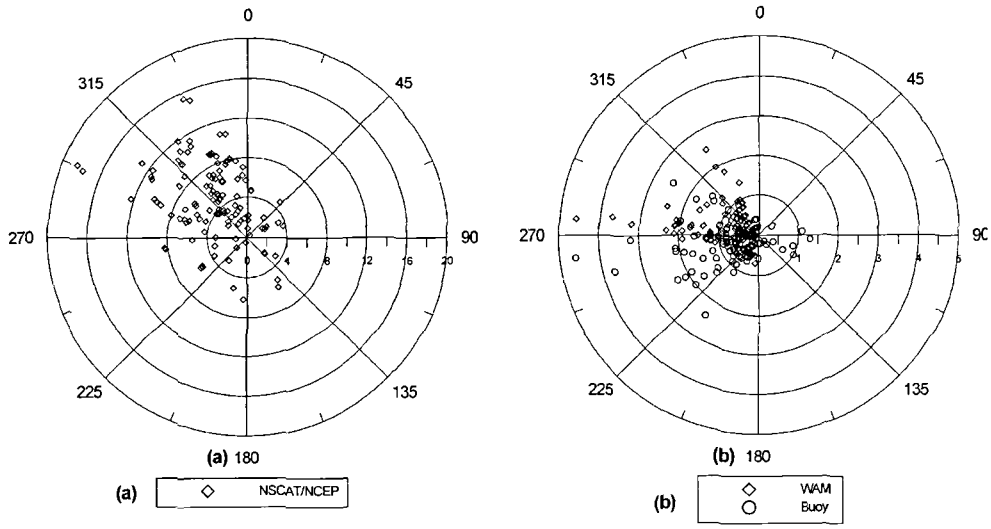

Fig. 6. Comparison of (a) *NSCAT/NCEP* blended wind direction and (b) *WAM* wave direction with *Buoy* wave direction off Duk-Juk.

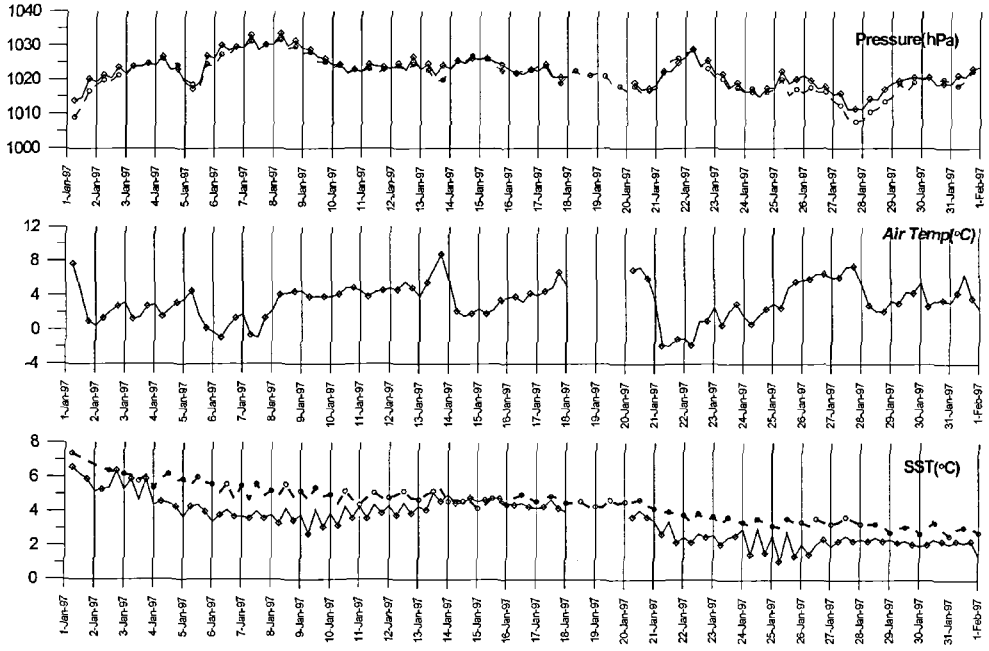

Fig. 7. Temporal distribution of (a) surface pressure, (b) air temperature and (c) SST off Chil-Bal and Duk-Juk.

This resulted in the surface pressure to 1028 hPa at "O". This study shows the buoy observation of pressure field matches with the movement of fast response of the synoptic features and the prevailing synoptic situation with reference to the two stations. The surface wave characteristics at these two locations are modulated by the fast response of the movement of the pressure systems prevailing on either side of the locations.

According to the theory on the growth of waves, energy transfer for wave growth takes place from the parametric region towards the discrete region

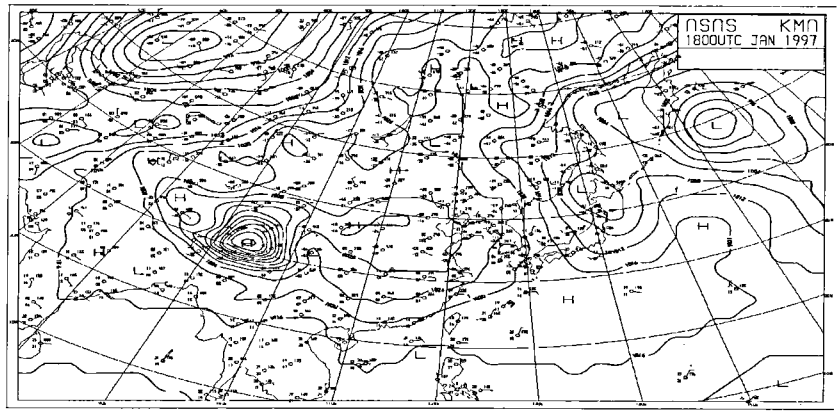

(a) 1800 UTC

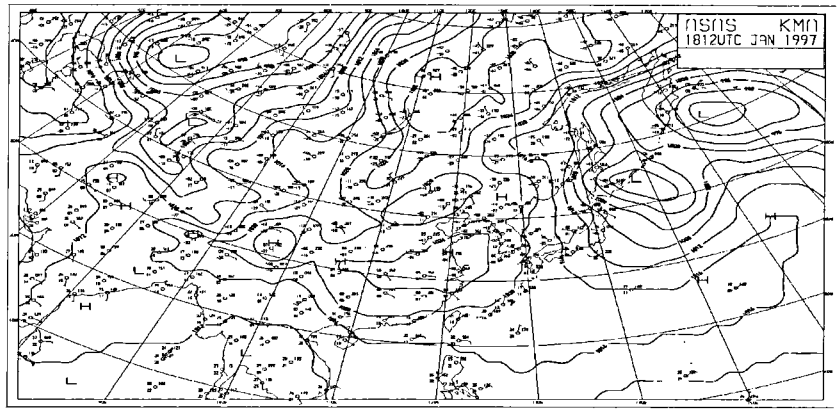

(b) 1812 UTC

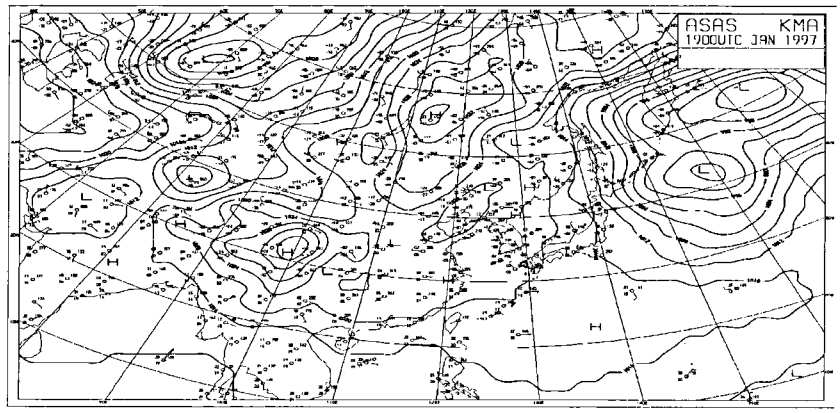

(c) 1900 UTC

Fig. 8. Synoptic charts of surface pressure distribution.

from the high frequency cut-off. The parametric region is the high frequency part and the discrete region lie in the low frequency part of the one-dimensional wave spectrum. The boundary between the parametric and discrete spectral domains is maintained at a fixed point and energy in each domain is conserved independently. In a growing wind sea, energy is initiated in the para-

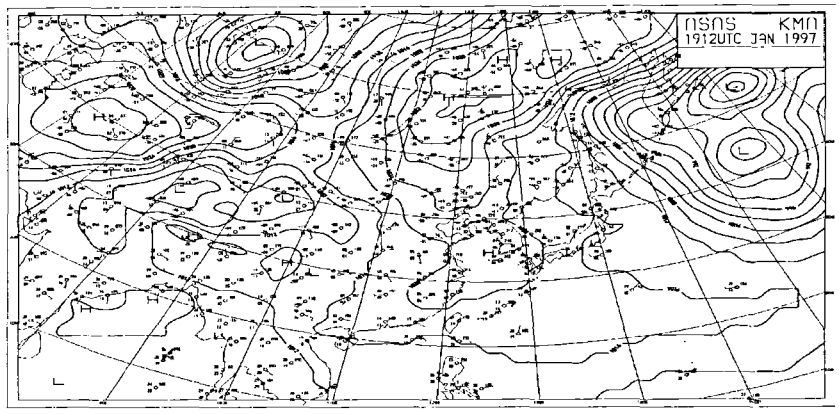

(d) 1912 UTC

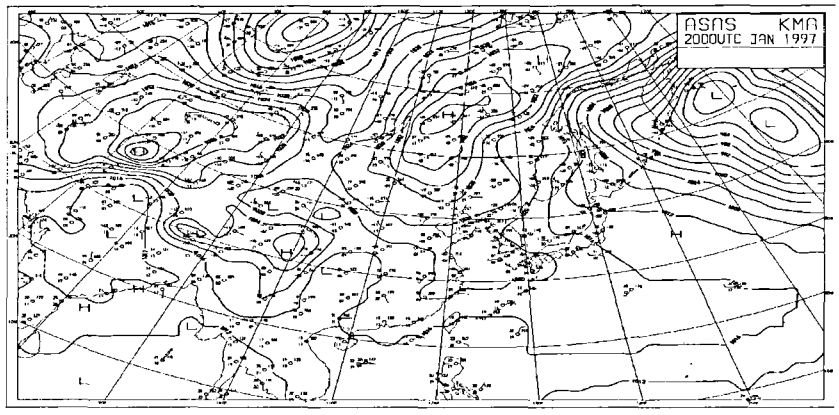

(e) 2000 UTC

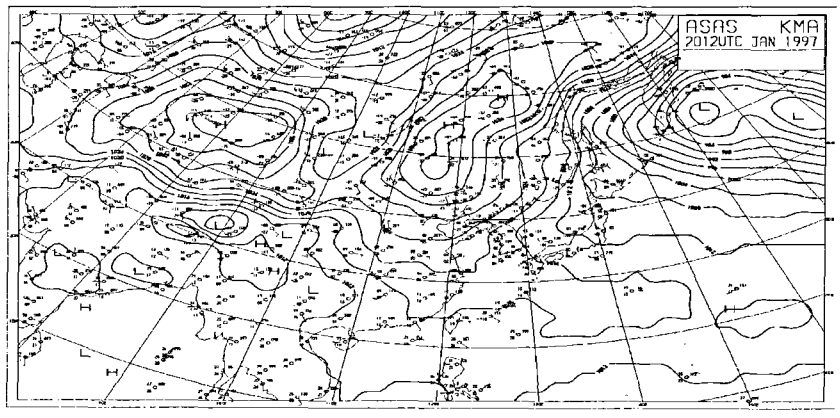

(f) 2012 UTC

Fig. 8. Continued.

metric region and the energy exchange occurs in the discrete region trigerring growth there. The wave growth in the wind sea region is halted when the non-dimensional peak frequency attains a value of 0.13. In a fully developed stage the growth rate decreases and non-linear interaction terms distribute energy to lower frequencies. Energy in the high frequency part of the spectrum is eventually

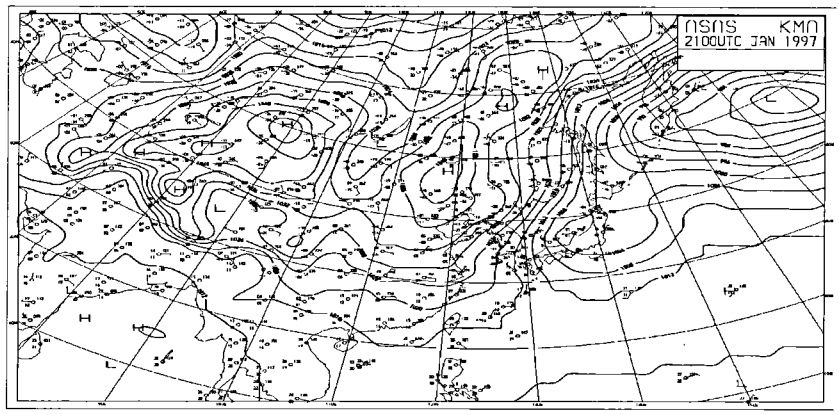

(g) 2100 UTC

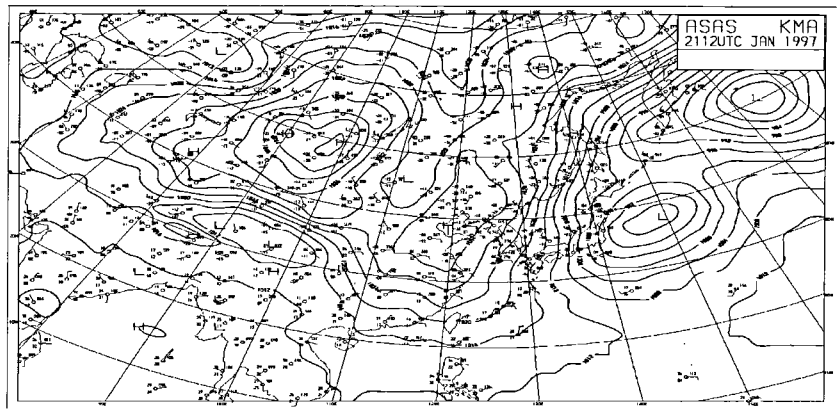

(h) 2112 UTC

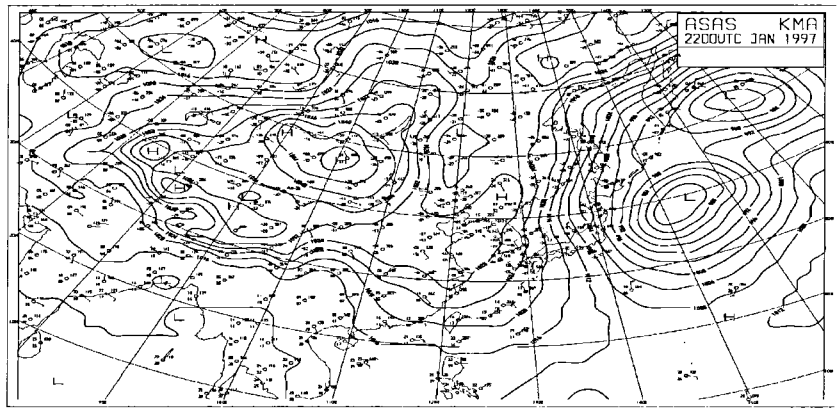

(i) 2200 UTC

Fig. 8. Continued.

allowed to dissipate. When the frequency is less than 0.13, waves propagate as swells. The temporal distribution of the peak spectral energy as a function of peak wave frequency off Duk-Juk and Chil-Bal is shown in Fig. 9 (a,b) and the corresponding swell energy is shown in Fig. 10 (a,b). The peak energy is dominant at both these locations on 1st January 1997 (associated with the

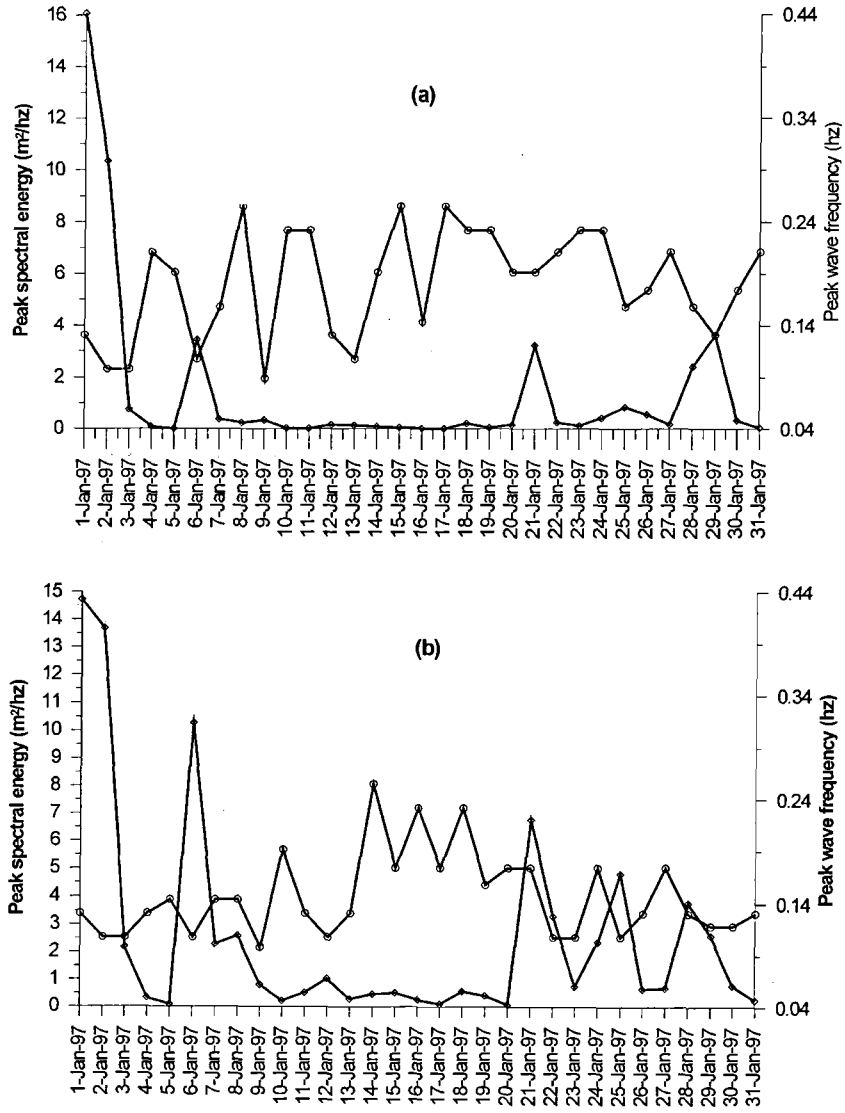

Fig. 9. Distribution of peak spectral energy (◇) and peak wave frequency (○) off (a) Duk-Juk and (b) Chil-Bal.

depression during end of December 1996). The corresponding peak wave frequency is centered at 0.1311 Hz both for Chil-Bal and Duk-Juk. It could be seen from Fig. 10 (a,b) the dominant swell peak energy on 2 January 1997 when the mean energy was dropping down. This is a typical situation which is found in extreme events, the domination of swell waves when the wind field recedes (Prasad, 2000). Both at Chil-Bal and Duk-Juk, the distribution in mean and swell peak energy is found the same trend as that of wave heights (Fig. 3 a,b). It is also seen in general that the high energy is associated with lower frequency. As advocated in spectral wave theory, if the wind speed increases the peak energy level is seen from the Fig. 9 migrating from the high frequency side to the low frequency part of the spectrum. As seen in Fig. 9 and 10, the relative energy level is high for the location Chil-Bal compared to Duk-Juk as a result of the bottom dissipation mechanism being the water depth at Duk-Juk is more shallow compared to Chil-Bal.

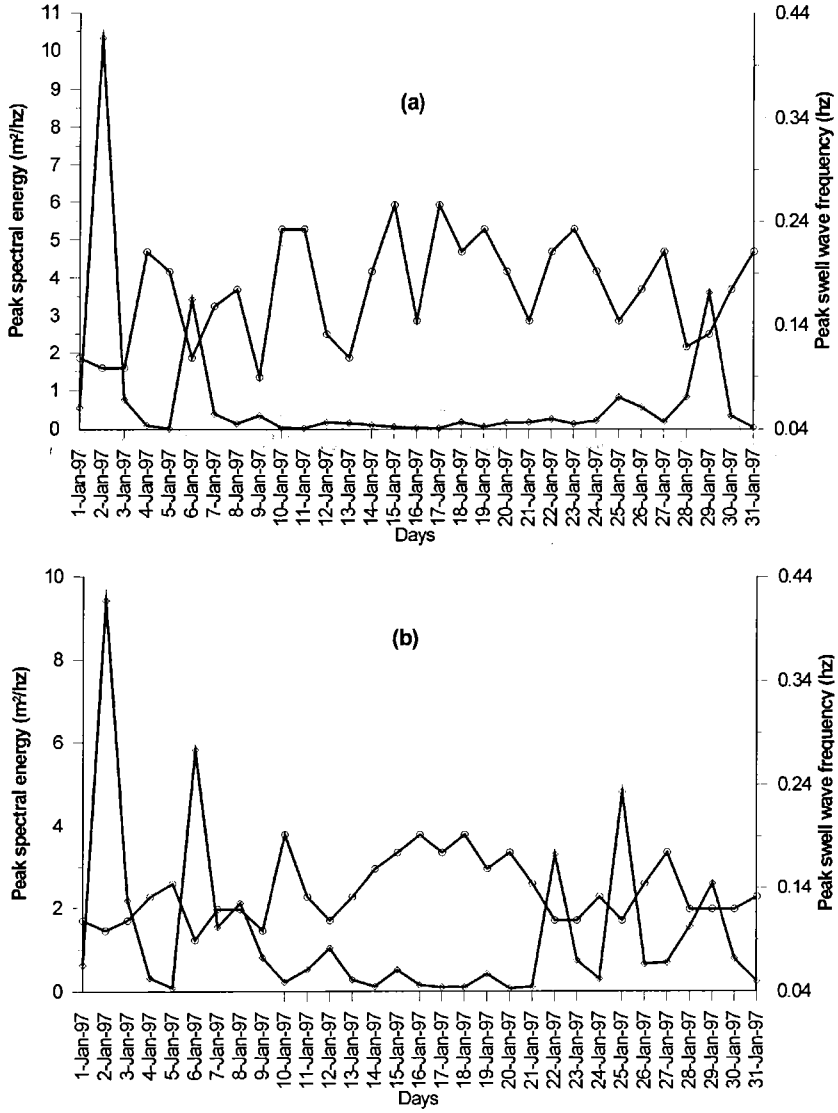

Fig. 10. Distribution of peak spectral swell wave energy (◇) and peak swell wave frequency (○) off (a) Duk-Juk and (b) Chil-Bal.

Conclusions

The model siumulation with WAM following validation with two shallow water buoy observations indicate the good performance of the wave model for the Korean seas. As known any wave model is highly sensitive on the accuracy of input wnd field, the blended NSCAT/ERS winds overlaid with NCEP analysis show an appreciable correlation with the observation. The oscillations which were seen in both the wind fields are to be further examined with detailed long term data to provide more insight for the cause of these oscillations. A proper knowledge on the periodicity of these observed oscillations will undoubtedly provide valuable information in improving the quality of existing wind forecast models in Korean context. The present work may be viewed as a contribution toward this goal.

Acknowledgments

The Department of Ocean Development, Government of India is acknowledged for funding the wave modelling effort at IIT Delhi. Cheju National University is acknoweldged for supporting a graduate student by Brain Korea 21 Project in 2002.

References

Chin, T.M., Milliff, R.F., and Large, W.G., 1998, Basin-scale, high-wave number sea surface wind fields from a multi-ressolution analysis of scatterometer data. Journal of Atmospheric and Oceanic Technology, 15, 741-763.

Elms, J.D., 1990, U.S. Navy regional climatic study of the Central east Asian coast and associated waters. U.S. Naval Oceanography Command Report. NAVAIR50-1C-556, 1990.

Ewing, J.A., 1971, A numerical wave prediction method for the north Atlantic Ocean. Deutch Hydrographic Zeitschriff, 24, 241-261.

Golding, B., 1983, A wave prediction system for real-time sea-state forecasting. Quarterly Journal of Royal Meteorological Society, 109, 393-416.

Groves, G.W. and Melcer, J., 1961, On the propagation of ocean waves on a sphere. Geophysical International, 8, 77-93.

Hasselmann, K., 1973, Measurements of wind wave growth and swell decay during the joint North sea wave project (JONSWAP). Deutch Hydrogrphic Zeitschriff, Reiche A12, 95.

Hasselmann, S. and Hasselmann, K., 1985, Computations and parametrizations of the nonlinear energy transfer in a gravity wave spectrum. Part I: A new method for efficient computations of the exact nonlinear transfer integral. Journal of Physical Oceanography, 15, 1369-1377.

Hasselmann, S., Hasselmann, K., Allender, J.H., and Barnett, T.P., 1985, Computations and parameterizations of the nonlinear energy transfer in a gravity wave spectrum. Part II: Parameterizations of the nonlinear energy transfer for application in wave models. Journal of Physical Oceanograaphy, 15, 1378-1391.

Komen, G.J., Cavaleri, M., Donelan, M., Hasselmann, K., and Janssen, P.A.E.M., 1994, Dynamics and Modelling of Ocean waves, Cambridge University Press, U.K., 554 p.

Komen, G.J., Hasselmann, S., and Hasselmann, K., 1984, On the existence of a fully developed windsea spectrum. Journal of Physical Oceanography, 14, 1271-1285.

Miles, J.W., 1957, On the generation of surface waves by shear flows. Journal of Fluid Mechanics, 3, 185-204.

Miles, J.W., 1960, On the generation of surface waves by turbulent shear flows. Ibid, 7, 469-478.

Milliff, R.F., Large, W.G., Morzel, J., Danabasoglu, G., and Chin, T.M., 1999, Ocean general circulation model sensitivity to forcing from scatterometer winds. Journal of Geophysical Research, Oceans, 104(C5), 11337-11358.

Pierson, W.J. and Moskowitz, L., 1964, A proposed spectral form for fully developed sea based on the similarity theory of S.A. Kitaigorodskii. Journal of Geophysical Research, 69(24), 5181-5191.

Prasad Kumar, B., Ruchi Kalra, Dube, S.K., Sinha, P.C., Rao, A.D., Raj Kumar and Abhijit Sarkar, 2000, Extreme wave conditions over the Bay of Bengal during a severe cyclone simulation experiment with two spectral wave models. Journal of Marine Geodesy, 23(2), 91-102.

Shemdin, O., Hasselmann, K., Hsiao, S.V., and Herterich, K., 1978, Nonlinear and linear bottom interaction effects in shallow water in turbulent fluxes through the sea surface, Wave dynamics and prediction, NATO Conference Series V, Plenum Press, 1, 647-665.

Snyder, R.L., Dobson, F.W., Elliot, J.A., and Long, R.B., 1981, Array measurements of atmospheric pressure fluctuations above surface gravity waves. Journal of Fluid Mechanics, 102, 1-59.

WAMDI group, 1988, The WAM model-A third generation ocean wave prediction model. Journal of Physical Oceanography, 18, 1775-1810.

Weller, R.A., Rudnick, D.L., Eriksen, C.C., Polzin, K.L., Oakey, N.S., Toole, J.W., Schmitt, R.W., and Pollard, R.T., 1991, Forced ocean response during the Frontal Air-sea Interaction experiment. Journal of Geophysical Research, 96(C5), 8611-8638.

Yuan, Y. and Jilan Su, 1984, Numerical modelling of the circulation in the East China Sea. In Ichiye T. (ed.): Ocean Hydrodynamics of Japan and East China Seas, Elsevier Science Publishers, 167-186.

Manuscript received, May 25, 2002
Revised manuscript received, August 20, 2002
Manuscript accepted, August 30, 2002